



## Assessment of the influence of electric arc furnace slag as a non-conventional filler for Nitrile Butadiene Rubber

Anna Gobetti<sup>a,\*</sup>, Giovanna Cornacchia<sup>b</sup>, Marco La Monica<sup>c</sup>, Annalisa Zacco<sup>d</sup>,  
Laura Eleonora Depero<sup>d</sup>, Giorgio Ramorino<sup>a</sup>

<sup>a</sup> Materials Science and Technology at Department of Mechanical and Industrial Engineering, University of Brescia, Via Branze 38, 25123, Brescia, Italy

<sup>b</sup> Metallurgy at Department of Mechanical and Industrial Engineering, University of Brescia, Via Branze 38, 25123, Brescia, Italy

<sup>c</sup> Laboratory for Resources Valorisation (RISE), Department for Sustainability, ENEA, Via Anguillarese 301, 00123, Roma, Italy

<sup>d</sup> Chemistry for Technologies Laboratory, INSTM and Department of Mechanical and Industrial Engineering, University of Brescia, Via Branze 38, 25123, Brescia, Italy

### ARTICLE INFO

#### Keywords:

Electric arc furnace slag  
Mechanical characterization  
Dynamic mechanical characterization  
Payne effect  
Crosslink density

### ABSTRACT

Reinforcement of polymers by the addition of particles filler is a complex phenomenon that depends mainly on the hydrodynamic effect and a complex interplay between polymer, filler, and interfacial region. Mineral fillers are usually adopted as low-cost extenders due to their lower cost.

In this study, the influence of a waste material such as electric arc furnace steel slag is assessed as filler for Nitrile-Butadiene Rubber following experimental procedures and analytical calculations adopted for traditional fillers. It was found that the slag content affects the static and the dynamic properties by increasing the material's capability to storage and dissipate energy. In addition to an important contribution of the hydrodynamic effect, the presence of an increasing immobilized rubber fraction around the slag particles (quantified by a differential scanning calorimetry analysis) plays a central role. The slag stiffens the NBR composite; the increase of static tensile and dynamic shear storage moduli was found to be consistent with the Halpin-Tsai and Guth-Gold prevision models respectively. Moreover, the non-linear dynamic behavior was found to be well-fitted by the Kraus equation models. The reinforcing ability of the slag particles as filler was confirmed by the negative slope of the Kraus plot on swelling data.

### 1. Introduction

Elastomers are important polymeric materials due to their exceptional elastic properties. However, for the many different practical applications, the addition of a reinforcement is essential to enhance the mechanical properties of these polymeric matrices [1–4]. Fillers are widely used in the rubber industry, as reinforcing, to facilitate the rubber production process or, to lower the final material cost [1]. Due to this, in rubber science and technology, the topic of rubber reinforcement can be considered one of the most important.

Reinforcement of polymers, by the addition of particles filler, is a complex phenomenon depending on numerous aspects including the hydrodynamic effect and an intricate interplay between the properties of the individual constituent phases: the polymer, the filler, and the interfacial region [5–8]. The actual reinforcement is deeply influenced by the arrangement of the particles which in the case of carbon black are

dispersed as fractal aggregates because of the surface activity of the particles that results in a filler-filler interaction. The filler-polymer interface is another significant factor affecting the macroscopic properties of filled polymers [9–11]. The existence of a rigid layer at the polymer-filler interface has been established by several authors [12–14]. Assuming a glass transition temperature gradient away from the particle interface, a mesoscale model to explain the reinforcement of elastomers in both linear and non-linear regimes (Payne effect) has been developed by Merabia et al. [15–17]. According to this model, the glassy layer formed around the filler particles is responsible for the reinforcement as it acts as a bounding agent between the particles, making its effect stronger when combined with the percolation of the filling network [15]. The fillers often used to modify the properties of NBR are mainly carbon black, silica, and fibers [16–19]. According to the reinforcing performance, the rubber fillers can be divided into reinforcing fillers and non-reinforcing fillers.

\* Corresponding author.

E-mail addresses: [a.gobetti@unibs.it](mailto:a.gobetti@unibs.it) (A. Gobetti), [giovanna.cornacchia@unibs.it](mailto:giovanna.cornacchia@unibs.it) (G. Cornacchia), [marco.lamonica@enea.it](mailto:marco.lamonica@enea.it) (M. La Monica), [annalisa.zacco@unibs.it](mailto:annalisa.zacco@unibs.it) (A. Zacco), [laura.depero@unibs.it](mailto:laura.depero@unibs.it) (L.E. Depero), [giorgio.ramorino@unibs.it](mailto:giorgio.ramorino@unibs.it) (G. Ramorino).

<https://doi.org/10.1016/j.rineng.2023.100987>

Received 13 January 2023; Received in revised form 16 February 2023; Accepted 24 February 2023

Available online 26 February 2023

2590-1230/© 2023 The Authors. Published by Elsevier B.V. This is an open access article under the CC BY-NC-ND license (<http://creativecommons.org/licenses/by-nc-nd/4.0/>).

In this context, the present research evaluates the influence of a waste material such as an electric arc furnace (EAF) steel slag as a filler in a Nitrile-Butadiene Rubber (NBR). Steel slag is the main scrap of the steel industry and consists of about 10–15% by weight of the produced steel [20–22]. Europe produces annually about 60 million tons of EAF slag so that it is needed to investigate new applications in order to promote the use rate of waste, conserve natural resources, and reduce landfilling. Since, according to Pisciotta [23], the chemical composition of EAF slag consists mainly of calcium oxide (CaO), silicon dioxide (SiO<sub>2</sub>), and iron oxides (FeO), it can be assimilated to natural effusive rocks of volcanic origin. This composition makes the EAF slag compliant to be reused as artificial aggregate in the building sector [24–26]. Nevertheless, unfortunately still a huge quantity is disposed of in landfills so the investigation of new applications is of fundamental relevance.

The EAF slag has been investigated for the first time as a filler in polymer matrices by Cornacchia et al., in 2015 [27]. Recently the EAF slag has been proposed as an alternative filler for epoxy screeds [28] and its influence was assessed also in elastomeric matrixes [29–31].

In this study, a commercial NBR has been filled with an increasing volume fraction of EAF slag in order to propose an alternative use of the main steel industry scrap as a low-cost filler for vulcanized rubber. The reinforcing effect of this new filler was evaluated following the same experimental procedures and analytical calculations adopted in evaluating the reinforcing effect of traditional fillers.

In particular, static and dynamic tests have been performed with the aim to assess the influence of the EAF slag as filler on tensile properties and dynamic behavior. The results showed that with increasing the filler presence the NBR composite stiffens; the increase of static tensile and dynamic shear storage moduli was found to be consistent with the Halpin-Tsai and Guth-Gold prevision models respectively. Moreover, the non-linear dynamic behavior was found to be well-fitted by the Kraus equation models [32,33]. The reinforcing ability of the slag particles as filler was evaluated by the swelling test, in particular, the crosslink density determined by the Flory-Rehner equation increased with the filler volume fraction and the Kraus equation [32,34] showed a reinforcing effect of EAF slag as filler.

The immobilized rubber fraction around the filler particles (bound rubber), has been quantified by differential scanning calorimetry (DSC) analysis [10].

In summary, the experimental results highlighted how an industrial waste such as the EAF slag can be valorized as secondary raw material for a dissimilar sector such as that of polymers with consistent environmental and economic benefits given by the avoided landfilling disposal and by the saving of virgin raw material. From a technical point of view, it was found that this non-conventional filler can be studied experimentally and via analytical modeling in the same way as other conventional fillers.

## 2. Experimental

### 2.1. Materials

The effect of EAF slag as filler for NBR has been evaluated on 4 different compounds added with different amounts of filler and the results have been compared to that of standard NBR. The vulcanized rubber used as matrix is a Nitrile Butadiene Rubber (NBR), nominal hardness 70 Shore A (carbon black 40 phr, sulfur vulcanized) provided by Novotema Spa (Villongo, Bergamo, Italy).

In summary, the tested compounds are:

- Standard NBR: the material is processed as supplied by the compounder only by compression molding. A certain amount of uncured rubber is placed as such between the two half-molds, which, when closed and heated, form and vulcanize it;
- EAF slag filled NBR at 0, 5, 10, 20, and 30% v/v is processed by calendaring followed by compression molding. A certain amount of

uncured rubber is calendared with EAF slag (from 0 to 30% v/v) in order to distribute and disperse the filler particles in the rubber matrix, then the obtained compound is placed as such between the two half-molds which, when closed and heated, form and vulcanize it. For safe of clarities, the calendaring would not be required for NBR 0% as it does not contain the slag as filler.

The slag was supplied by the company ASONEXT Spa (Ospitaletto BS, Italy) steelmaking plant. The slag in use in this research has been produced by a specific system named Slag-Rec [35,36] for dry granulating EAF molten slag. This technique allows to keep the slag phase transformations and final mineralogical constitution under control. The slag employed as filler in the elastomeric matrix has been ground by manual pulverizing mill for a grinding time of 25 s for each 100 g of slag.

The pulverized EAF slag has been sieved to exclude particles larger than 106 µm (sieve mesh 140).

### 2.2. Methods

#### 2.2.1. EAF slag characterization

**2.2.1.1. X-ray fluorescence spectroscopy (XRF).** The X-ray fluorescence was used to determine the chemical composition of the EAF slag which is reported in Table 1.

**2.2.1.2. X-ray diffraction (XRD).** Crystalline phases identification of the slag was carried out by XRD analysis performed by a diffractometer equipped with an X'Celerator detector and Cu anode (CuKα = 0.15406 nm), operating at 40 kV and 40 mA, on pulverized and sifted slag. In Fig. 1 the X-ray diffraction pattern of the slag sample [37] is shown.

**2.2.1.3. Scanning electron microscope (SEM-EDXS) analysis.** Another useful technique useful for the morphological and elemental analysis of the phases is the analysis performed by Scanning Electron Microscopy (SEM) integrated with Energy Dispersive X-ray Spectrometry (EDXS) [38]. The EAF slag sample was analyzed after being polished. In Fig. 2 the SEM-EDXS analysis carried out on a metallographically polished sample utilizing back-scattered electron (BSE) mode is reported.

**2.2.1.4. Leaching behavior.** The leaching of Molybdenum, Chromium, and Vanadium has been determined in accordance with the standard CEN - EN 12457-2 [39]. For this analysis the slag has been ground by a mortar and successively sieved to obtain a grain size <4 mm. The leachates have been analyzed by an Avio 200 ICP Optical Emission Spectrometer to measure the concentration in the solution Cr, Mo, and V.

Since it was found that the slag grain size affects its leaching behavior [40], the leaching test was performed also on free EAF slag of a grain size lower than 106 µm in order to evaluate the shielding capability of the rubber matrix that incorporates the filler. The leaching of standard NBR and an EAF slag block completely incorporated in NBR were also performed. The results of the leaching test are given in Fig. 3.

#### 2.2.2. EAF slag filled NBR characterization

**2.2.2.1. Tensile test.** Mechanical tensile tests were performed at room temperature and a cross-head rate of 100 mm/min on test pieces of 50 mm length (distance between the grips of about 30 mm) and 4 mm width according to the standard ISO 37:2017 type 2 [41].

**2.2.2.2. Scanning electron microscope (SEM) analysis.** The morphology and distribution of slag particles in the NBR composites were assessed by SEM observations of cross-sections of specimens broken in liquid nitrogen after coating the surface with sputtered gold.

**Table 1**

First line: EAF slag chemical composition determined by X-ray fluorescence spectroscopy; all amounts are reported in wt%. Second line: different basicity indexes.

SiO <sub>2</sub>	Al <sub>2</sub> O <sub>3</sub>	Fe <sub>2</sub> O <sub>3</sub>	MnO	CaO	MgO	P <sub>2</sub> O <sub>5</sub>	TiO <sub>2</sub>	Cr <sub>2</sub> O <sub>3</sub>	S	Na <sub>2</sub> O	K <sub>2</sub> O	F
9.5	7.6	40.2	5.6	29.8	3.6	0.5	0.4	2.3	0.1	0.4	[/]	[/]
<b>Basicity</b>		<b>CaO/Al<sub>2</sub>O<sub>3</sub></b>		<b>Al<sub>2</sub>O<sub>3</sub>/SiO<sub>2</sub></b>		<b>IB2 CaO/SiO<sub>2</sub></b>		<b>IB4 (CaO+MgO)/(SiO<sub>2</sub>+Al<sub>2</sub>O<sub>3</sub>)</b>				
0.6		3.9		0.8		3.2		2.0				

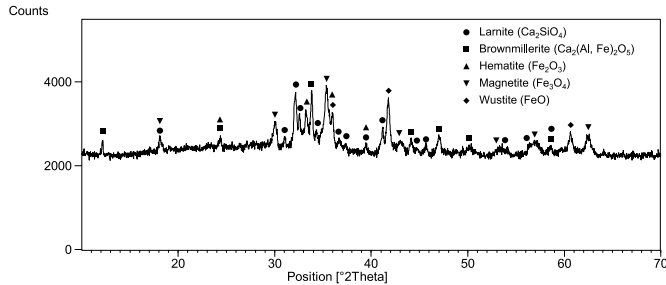


**Fig. 1.** X-ray diffraction pattern collected from EAF slag sample and crystalline phases identification. (ICDD reference numbers: 00-033-0302 Larnite; 00-030-0226 Brownmillerite; 01-084-0308 Hematite; 01-079-0418 Magnetite; 01-077-2355 Wustite).

**2.2.2.3. Dynamic mechanical analysis (DMA).** Rectangular specimens (nominal dimension 8 × 4x2mm) were cut from the rubber sheets.

Dynamic mechanical tests were performed in the shear sandwich configuration and frequency of 1 Hz with increasing shear strain amplitude (between 0.02 up to the maximum applicable strain, according to the machine bearing capabilities of 18 N). For each test, at least three repetitions were performed.

**2.2.2.4. Swelling.** For the swelling test rectangular samples of about 500 mg (m<sub>0</sub>) were cut and immersed in toluene in sealed glass tubes for 48 h at room temperature. The samples were then weighed (m<sub>s</sub>) and dried in an oven with a suction system at 80 °C for 48 h before being weight again (m<sub>d</sub>). The swelling coefficient is determined as shown in Equation (1):

$$\text{Swelling coefficient } [\%] = \frac{m_s - m_0}{m_0} \frac{1}{\rho_s} \quad (1)$$

Where ρ<sub>s</sub> is the density of the swelling agent, i.e. toluene 0.867[g/cm<sup>3</sup>].

The equilibrium swelling index is determined by crosslink density and the attractive forces between solvent and polymer. The theoretical extent of swelling is predicted by the Flory–Rehner equation [42–44] (Equation (2)):

$$\nu = - \frac{\ln(1 - v_{Rf}) + v_{Rf} + \chi v_{Rf}^2}{v_{Rf}^{1/3} - \frac{2v_{Rf}}{f}} \frac{1}{V_s} \quad (2)$$

where:

ν is the crosslink density [mol/cm<sup>3</sup>].

V<sub>s</sub> = 106.52 (m<sup>3</sup>/mol) is the toluene molar volume;

f = 4 for tetra functional network junctions;

χ is the Flory–Huggins solvent–polymer interaction parameter;

v<sub>Rf</sub> is the volume fraction of elastomer in the swollen mass, determined according to Ellis and Welding equation [4] Equation (3).

$$v_{Rf} = \frac{\frac{w_2}{\rho_s}}{\frac{w_2}{\rho_s} - \frac{w_1}{\rho_s}} \quad (3)$$

where:

w<sub>2</sub> is the weight fraction of the compound in the swollen specimen;

w<sub>1</sub> is the weight fraction of the solvent in the swollen specimen;

ρ<sub>s</sub> is the density of the swelling agent;

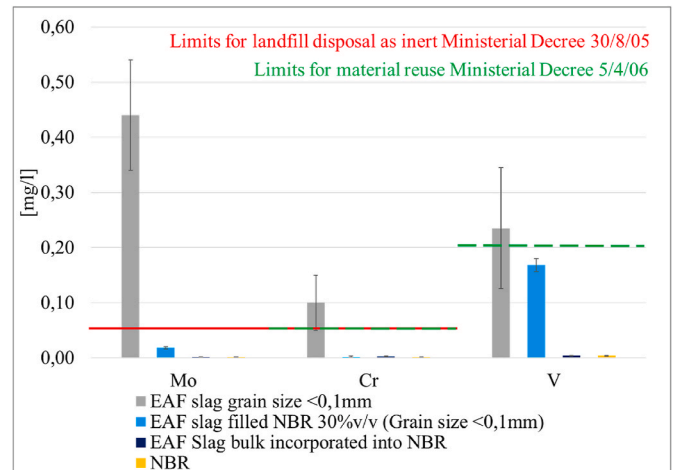


**Fig. 3.** Leaching test CEN EN 12457–2 results of EAF slag (grain size < 4 mm), free EAF slag, NBR filled with EAF slag at 30%v/v (grain size <106 μm), EAF slag block incorporated into NBR and standard NBR.

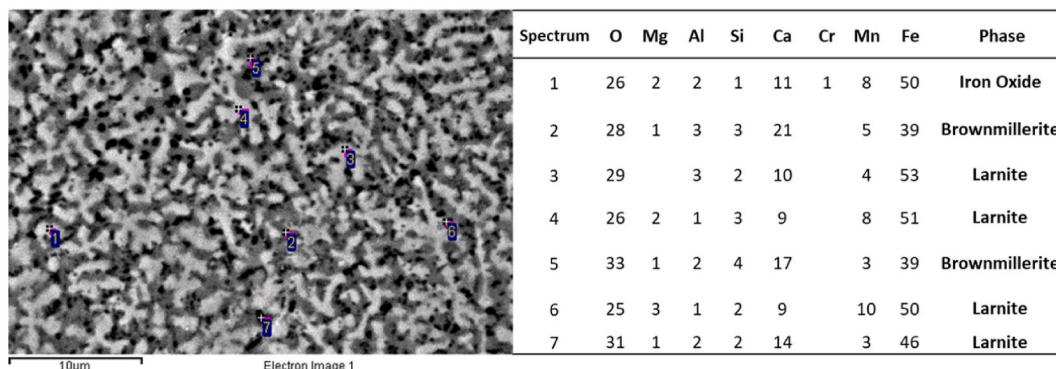


**Fig. 2.** SEM back-scattered electron (BSE) image of slag microstructure [%wt] with its EDXS analysis on a metallographically polished sample.

$\rho_c$  is the compound density.

The Flory–Huggins solvent–polymer interaction parameter is equal to 0.36 and it has been determined from the Bristow and Watson semi-empirical equation [45–47].

The properties of filled elastomers are linked to the interaction between filler and matrix which can be theoretically estimated by the Kraus equation [34,48] (Equation (4)):

$$\frac{v_{R0}}{v_{Rf}} = 1 - K \left( \frac{\varphi}{1 - \varphi} \right) \quad (4)$$

where:

$\varphi$  is the filler volume fraction;

$K$  is the polymer-filler interaction parameter;

$v_{Rf}$  is the elastomer volume fraction;

$v_{R0}$  is the rubber gum vulcanizate volume fraction, assumed to be equal to  $v_{Rf}$  of Standard NBR (no added EAF Slag).

**2.2.2.5. Differential scanning calorimetry.** The calorimetric glass transition was determined by differential scanning calorimetry (DSC). The sample is cooled from room temperature to  $-90^\circ\text{C}$  at  $10^\circ\text{C}/\text{min}$  and maintained for 60 min. The measurement is then carried out during subsequent heating at  $10^\circ\text{C}/\text{min}$ . DSC analysis is performed twice.

The heat flow [mW] is converted to heat capacity ( $C_p$  [J/(g $^\circ\text{C}$ )]). NBR composites samples consist of a weight fraction of filler and a weight fraction of polymer; since only the latter is responsible for the variations associated with the glass transition, the heat capacity has been normalized to the polymer fraction as shown in Equation (5):

$$C_p^* = \frac{C_p}{1 - \text{filler (\%wt)}} \quad (5)$$

Where  $C_p$  is the heat capacity associated with the composite,  $C_p^*$  is that associated with the polymer fraction. The filler weight fraction is determined by thermogravimetric analysis (TGA) ( $10^\circ\text{C}/\text{min}$ ,  $25$ – $550^\circ\text{C}$  in Nitrogen atmosphere and  $550$ – $800^\circ\text{C}$  in Oxygen atmosphere).

The heat capacity increment,  $\Delta C_p^*$  as a measure of the amount of polymer which participates in the glass transition is dependent on the intermolecular rigidity, that is, the polymer–filler interaction in the filled rubber [10].  $\Delta C_p^*$  is determined in a temperature range of  $\pm 2.5^\circ\text{C}$  with respect to the glass transition temperature ( $T_g$ ). The dependency  $\Delta C_p$  on intermolecular rigidity is often evaluated in terms of immobilized polymer chains in the composites. The fraction of immobilized polymer is calculated by Equation (6) [49]:

$$\text{Immobilized rubber fraction [\%]} = 1 - \frac{\Delta C_p^*}{\Delta C_p^0} \quad (6)$$

where  $\Delta C_p^0$  is assumed to be the heat capacity variation of standard NBR.

### 3. Results and discussion

#### 3.1. EAF slag characterization

##### 3.1.1. X-ray fluorescence spectroscopy results

The chemical composition of the EAF slag determined by X-ray fluorescence spectroscopy is reported in Table 1.

The ratio between the percentage of basic and acidic components (basicity index IB) allows to express and to interpret important metal-slag balances, such as oxidizing power of slag, the balance of desulfurization, and dephosphorization, metal-slag distribution of manganese. The simplest expression of the basicity index, by means of the ratio between the weight percentages of CaO and SiO<sub>2</sub>, is IB<sub>2</sub>, here equal to 3.2. IB<sub>2</sub> does not consider the presence of other components with acidic or basic behavior, so it is possible to define the complete basicity factor with IB<sub>4</sub> parameter, calculated as ratio between principal basic oxides (CaO+MgO) and main acid oxides (SiO<sub>2</sub>+Al<sub>2</sub>O<sub>3</sub>). The basicity of the

slag is required in the steelmaking process in order to preserve the integrity of the refractories, which are also basic, for as long as possible. Moreover, the slag chemical composition is related also to the leaching of heavy metals; in turn, it is affected by the cooling conditions adopted in the slagging phase. A rapidly cooled slag is prone to form a glassy phase which shields the heavy metals and prevents them from leaching [50,51]. It was observed by Tossavainen et al. [51] that if the basicity factor IB<sub>4</sub> is greater than 1, as in the EAF slag object of this study (see Table 1), it is possible to affirm that the glassy phase formation occurred leading a heavy metal leaching prevention.

##### 3.1.2. X-ray diffraction results

Fig. 1 shows the X-ray diffraction (XRD) pattern and the crystalline phases identification of the slag sample. From these results, it was possible to notice that the main detected crystalline phases are Larnite (Ca<sub>2</sub>SiO<sub>4</sub>), Brownmillerite (Ca<sub>2</sub>(Al, Fe)<sub>2</sub>O<sub>5</sub>), and iron oxides in the mineralogical forms of Hematite (Fe<sub>2</sub>O<sub>3</sub>), Magnetite (Fe<sub>3</sub>O<sub>4</sub>) and Wustite (FeO). These results are in accordance with the chemical composition reported in Table 1 which shows a massive presence of iron and calcium.

##### 3.1.3. SEM/EDS analyses

Fig. 2 shows the SEM-EDXS analysis of a metallographically polished sample using back-scattered electron (BSE) mode. The exact mineralogy identification is difficult because some slag phases have varying contents of substituted ions. Moreover, the slag studied in the present work was obtained by a rapid cooling process, that allows to obtain a very fine phase distribution to reduce the intrinsic heterogeneity of the slag but on the other side makes the identification of the phases more difficult by SEM/EDXS analysis due to the fine available areas. Nevertheless, thanks to the comparison with the two analytical techniques used, it was possible to classify the main phases present, namely Iron Oxides identified by the XRD as Wustite (FeO), Hematite (Fe<sub>2</sub>O<sub>3</sub>), and Magnetite (Fe<sub>3</sub>O<sub>4</sub>) containing a small quantity of Cr, Ca, Si, Mg, Mn, and Al. Both analyses detected the presence of Larnite (Ca<sub>2</sub>SiO<sub>4</sub>) and Brownmillerite (Ca<sub>2</sub>(Al, Fe)<sub>2</sub>O<sub>5</sub>) with the presence of other elements in small quantities.

##### 3.1.4. Leaching test

Fig. 3 shows the concentration of Molybdenum, Chromium, and Vanadium in the leachates detected by ICP of EAF slag (grain size <4 mm in accordance with the standard CEN EN 12457–2 [39]) and EAF slag (grain size <106 μm) both free and incorporated into the NBR matrix at 30%v/v.

From the comparison between slag and composite at equal grain size, it can be noted that the concentration of Mo, Cr, and V in the eluate is lower when the slag particles are incorporated into the rubber matrix (especially Mo and Cr). The shielding effect of the rubber is evident in the leaching of the monolithic slag completely embedded in the rubber which shows virtually no release just like NBR alone.

For the sake of clarity, it is important to underline that the slag incorporated in the rubber is not the same tested as the free slag, however, the inertizing effect of the polymer matrix is attributable to the hydrophobicity of NBR. As last, it was found that the leaching behavior is affected by the slag grain size, especially for Mo leaching which for fine slag is almost twice than for coarse slag. The correlation between the slag grain size and its leaching behavior was confirmed by several literature studies [40,52–54].

#### 3.2. EAF slag filled NBR characterization

##### 3.2.1. Tensile properties

Fig. 4 shows a representative tensile test stress-strain curve for each compound. From these curves the main tensile properties such as stress at break, strain at break, and Young's modulus are determined.

Tensile test results show a reduction of the stress at break of about 65% between standard NBR and NBR filled with EAF slag 30%v/v, while

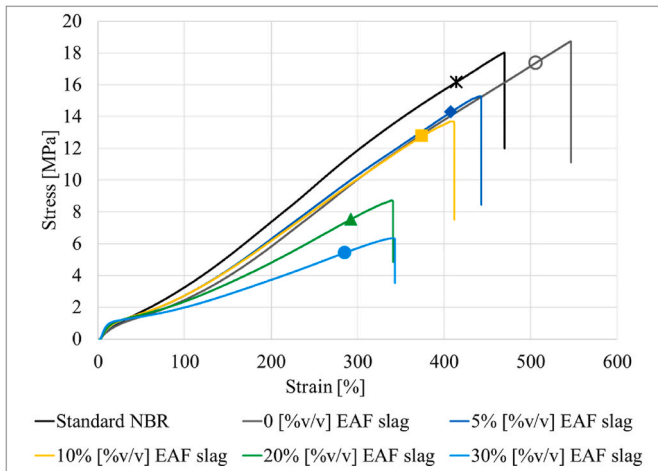


Fig. 4. Stress-optical strain curves of a representative sample for standard NBR and compound filled with 0,5,10, 20, 30% of EAF slag.

the reduction of the strain at break is about 30%. It is possible to state that the elongation at break and the stress at break are significantly reduced for filler quantities exceeding 10% v/v. The calendering process has the effect of increasing both elongation at break (by about 15%) and stress at break (by about 5%). This is due to better dispersion and distribution of the carbon black in the compound as evidenced by SEM observations (see 3.2.2 Morphology and distribution filler particles) that likely reduce the fraction of occluded rubber. Similar results were found in Refs. [55,56]. Furthermore, it is possible to note that standard NBR at large deformations (>100%) and up to failure presents greater stress than the same compound subjected to the calendering process (named 0% [v/v] EAF slag) at the same deformation. This results in a higher secant elastic modulus at large strain. The calendering process implies a double effect on the material: on one side it improves the ultimate tensile properties by a better dispersion and distribution of the carbon black, on the other hand, it softens the compound as it dissolves the macromolecular structure. The compound stiffening due to the presence of EAF slag as filler is clearly appreciable in Young's modulus value as shown in Fig. 5. Compared to the influence of other fillers on a comparable NBR matrix, it was found that the influence of a presence of 20% [v/v] of EAF slag (equal to 14%wt) results in a stress at 300% strain equal to 10 MPa and in stress at break of about 15 MPa. These values are higher than that found by Wang et al. for a presence of 14%wt of nano-Fe<sub>3</sub>O<sub>4</sub> where the stress at 300% strain and the stress at break are

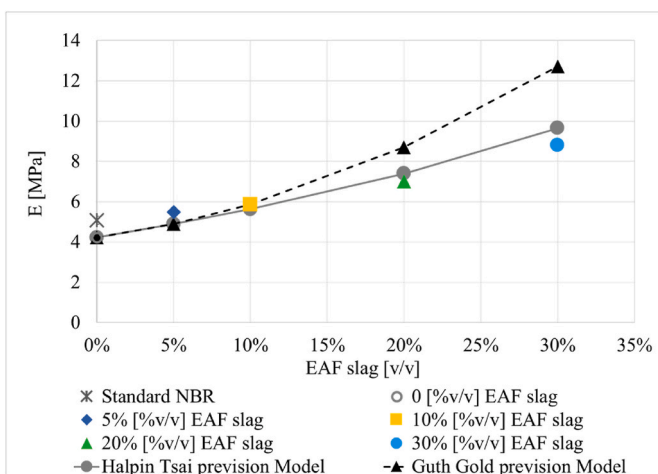


Fig. 5. Experimental and theoretical Young's modulus as a function of EAF slag as filler [%v/v].

about 4.5 and 22 respectively [57]. On the other side, the strain at break reduction is lower for nano-Fe<sub>3</sub>O<sub>4</sub> (5%) compared to that of slag (18%).

The effect of particle reinforcement was also evaluated using analytical models. Guth-Gold and Halpin-Tsai equations have been used to predict the tensile modulus of NBR composites (see Fig. 5) under the approximation of spherical particles. In the following calculation, the considered filler is only the EAF due to its greater size and content with respect to fillers present in standard NBR. Guth and Gold [50,58] proposed a quadratic term to explain the reinforcement effect of spherical fillers on elastomers, as shown in Equation (7):

$$E = E_m (1 + 2.5\varphi + 14\varphi^2) \quad (7)$$

Where  $E$  and  $E_m$  are the Young's moduli of NBR filled with different EAF slag volume fractions ( $\varphi$ ) and calendered NBR with no EAF slag added respectively.

Halpin-Tsai equation has been also used to investigate the reinforcement effects of filler in composite materials. Normally this model is used to predict the modulus for aligned fiber composites, but it has been used before to predict the modulus of nanocomposites [59]. The studied NBR composites filled with EAF slag are not nanocomposites due to the greater size of filler particles, nevertheless, it was found a good experimental data prevision. Halpin-Tsai equation is reported in Equation 8

$$E = \frac{E_m(1 + \zeta\eta\varphi)}{1 - \eta\varphi} \quad (8)$$

Where  $\zeta$  is a filler shape factor which is 2 for spherical particles and  $\eta$  is taken as unity.

In Fig. 5 the experimental and the theoretical Young's modulus is reported as a function of EAF slag volume fraction. Experimental data show that the modulus increases with slag volume fraction up to double for a filler presence of 30% v/v. The NBR composites stiffening could be attributed to two factors: the bound rubber content and the hydrodynamic effect. The bound rubber may be defined as the polymer layer adherent to the filler particles which is stiffer than the bulk polymer. With increasing the filler volume fraction the immobilized rubber fraction around the filler particles (bound rubber) increases (see 3.2.5 Differential scanning calorimetry analysis) causing also an increment of the crosslink density [2,60] (see 3.2.4 Crosslink density).

It was found that for EAF slag volume fraction up to 20%, both theoretical models well predict the experimental data, while for NBR filled with 30%v/v the Halpin-Tsai model reveals to better fit experimental data.

In the tensile test, it emerged an increase in the elastic modulus and at the same time a reduction in the stress and strain at break. This behavior is well-known for mineral fillers, and it is related to reduced polymer network mobility due to the presence of an increasing amount of rigid particles. On one side, the mobility reduction results in a material stiffening at low strain but, on the other side, with increasing the applied strain the slag filled materials show lower mechanical properties. This is a consequence of the limited mobility of the macromolecular network, which when is free to orient itself in the direction of the maximum applied stress manages to distribute the load homogeneously results, at macroscopic level, in higher mechanical properties. When the rigid particles hinder the orientation, the load is no longer distributed homogeneously but localized over stresses are created. At a macroscopic level this results in a reduction of the global stress and strain at failure. In this context, the filler-matrix interaction is very important as a strong adhesion between filler and matrix, allows the elastomeric matrix to transfer the load to the filler increasing the global mechanical properties (as occurs for the reinforcing fillers).

The stress at break reduction with increasing the amount of filler above a small filler percentage by weight (less than 5%) was found also by Kumarjyoti et al. [61] and Wang et al. in their study on mechanical properties of nano-Fe<sub>3</sub>O<sub>4</sub> or nano-SrO-6Fe<sub>2</sub>O<sub>3</sub> reinforced NBR [57,62].

The practical advantages related to the stiffening effect of the EAF

slag as a low-cost non-conventional filler are detailed in a previous study [31]. In particular, NBR is a rubber compound extensively used for gaskets production that mainly works in compressive configuration (typically in sealing systems) where a stiffer compound results in improved sealing system performances thanks to higher contact pressure (sealing in displacement control) or lower deformation (sealing in load control) that implies lower stress relaxation. Beyond the technical aspects, the obtained results showed that the influence of slag as filler is comparable to that of conventional non-reinforcing fillers so that an industrial waste such as slag can be used instead, with consequent economic and environmental benefits.

### 3.2.2. Morphology and distribution of filler particles

Fig. 6 shows SEM images of the fracture surface of all material investigated broken in nitrogen. Fig. 6 a) and b) show the micrograph of standard NBR and calendered NBR without EAF slag (0%[v/v] EAF slag) in order to assess the influence of the calendaring process on the distribution and dispersion of carbon black in NBR. It is possible to note that some carbon black agglomerates are observable in standard NBR (Fig. 6 a)), while the filler dispersion is noticeably improved in calendered NBR. Regarding the EAF slag filled NBR composites (Fig. 6 b-f)) in the backscattering SEM images, a good filler distribution and dispersion are evident. In particular, it is possible to observe a better filler particles

incorporation for slag particles of size lower than 50  $\mu\text{m}$ . In fact, in the micrographs, at the edges of the larger particles, there seems to be a small gap given by a lower cohesion between the filler and the matrix. This means that a smaller particle size of the filler leads to better incorporation into the matrix, but on the other hand in the case of the slag, it also involves high grinding costs, so it is necessary to find a compromise. Among the size of EAF slag particles, another important aspect is the particle shape: generally, the larger particles show acute angles which in an elastomeric matrix lead more easily to the initiation of a crack by decohesion due to a triaxiality of the stresses. The reinforcing effect of EAF slag particles smaller than 106  $\mu\text{m}$  was evaluated by the Kraus plot (see 3.1.5 Crosslink density) and it was found to be good due to the negative slope of the obtained curve.

### 3.2.3. Dynamic properties

In real applications rubber products often work in cyclic conditions so that dynamic properties allow to assess the correlation between the rubber's viscoelastic behavior to its performance in service life. Under dynamic conditions, a rubber assimilates energy which is in part stored, as in an ideal solid (usually modeled as a spring associated with the elastic (or storage) modulus  $G'$ ); and in part, it is dissipated by internal friction, as in an ideal fluid (usually modeled as a dashpot associated to is the viscous (or loss) Modulus  $G''$ ) [60,63]. The ratio of the energy

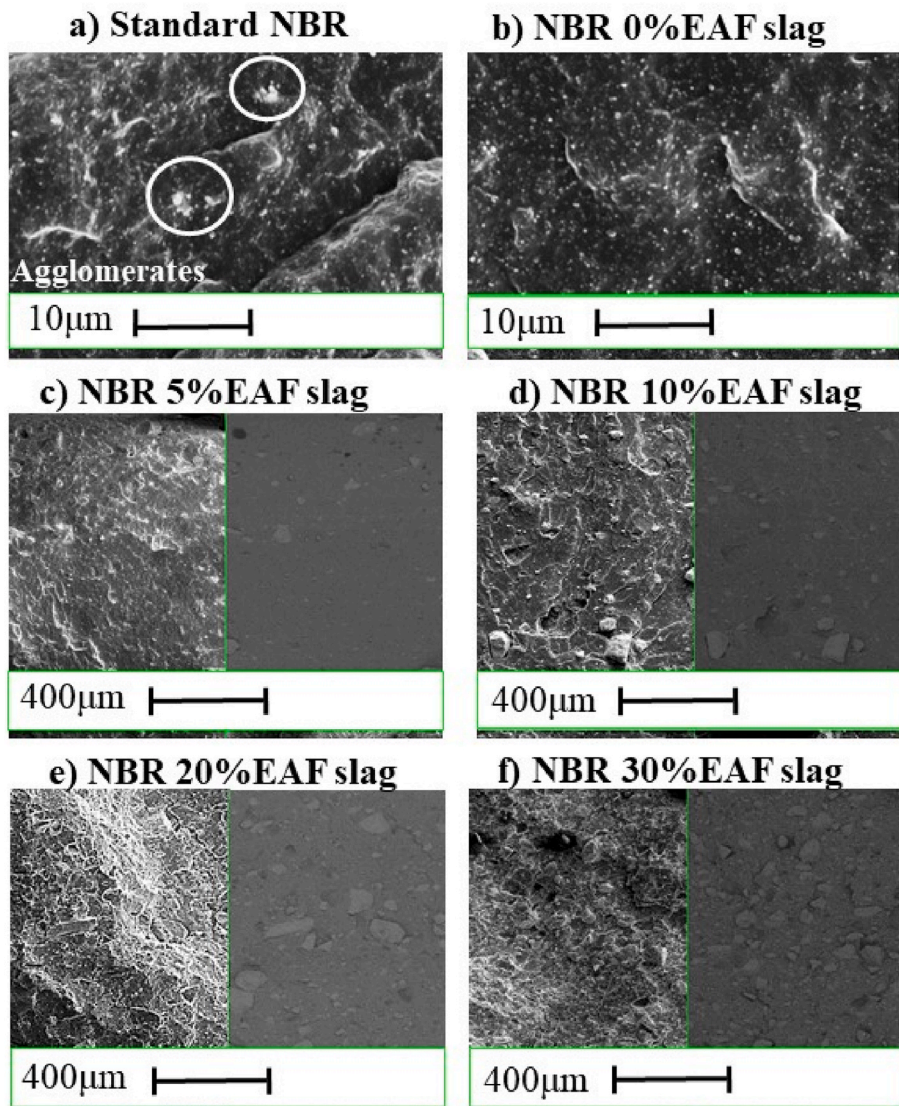


Fig. 6. SEM micrograph and backscattering images of cross sections of specimens broken in liquid nitrogen. a) micrograph of standard NBR; b) micrograph of calendered NBR filled with 0% EAF slag; c) micrograph and backscattering images of calendered NBR filled with EAF slag at 5%v/v; d) micrograph and backscattering images of calendered NBR filled with EAF slag at 10%v/v; e) micrograph and backscattering images of calendered NBR filled with EAF slag at 20%v/v; f) micrograph and backscattering images of calendered NBR filled with EAF slag at 30%v/v.

dissipated to the energy stored is a function of the viscoelastic properties, the temperature, the strain amplitude, and the strain rate.

The addition of reinforcing fillers to elastomeric materials increases, stiffness as well as tensile and tearing resistance which, on the other side, is often associated with a strain at break reduction [64]. The presence of filler strongly influences also the low amplitude dynamic properties [64–73]. The dynamic moduli behavior of unfilled rubber follows the classical theory of linear viscoelasticity [72,73] and the classical time/temperature superposition principle can be used [63]. The filled rubber dynamic modulus dependence on the strain amplitude is known as the “Payne effect” [74–77]. The storage modulus shows a plateau at a low strain amplitude and then it decreases with increasing the strain amplitude up to a high strain plateau value.

The Payne effect has been the subject matter of several theories which can be classed into two main types: filler structure models and matrix–filler bonding and debonding models [2]. However, there are two other factors that govern the conservative modulus but unlike the previous ones, they are independent of the amplitude of the shear stress: the hydrodynamic effect and the rubber network [78].

Payne [17,79] stated that the strain amplitude influence on dynamic moduli is related to the agglomeration and de-agglomeration of the filler network, and for carbon black filled elastomers, the rigidity of the structure depends on the rigidity of the filler–filler bonds. Under these assumptions, both the storage and loss moduli dependencies on the strain amplitude, have been modeled by Kraus [33] (Equation (9) and Equation (10)).

$$G'(\gamma) = G'_{\infty} + \frac{G'_0 - G'_{\infty}}{1 + \left(\frac{\gamma}{\gamma_c}\right)^{2m}} \quad (9)$$

$$G''(\gamma) = G''_{\infty} + \frac{2(G''_m - G''_{\infty})\left(\frac{\gamma}{\gamma_c}\right)^m}{1 + \left(\frac{\gamma}{\gamma_c}\right)^{2m}} \quad (10)$$

where  $\gamma_c$  is the strain amplitude in correspondence with which the loss modulus achieves its maximum  $G''_m$ .  $G'_0$  is the storage modulus at low strain amplitudes (lower than 0.01%);  $G'_{\infty}$  and  $G''_{\infty}$  are the asymptotic plateau values of the storage and loss modulus at high strain amplitudes, respectively;  $m$  is a non-negative phenomenological exponent to fit the experimental data [48,71]. Within the filler aggregation models, the concept of occluded rubber is often introduced [80,81]. Under increased applied strain, the trapped matrix is less and less shielded so that the dynamic properties are affected by the immobilized rubber fraction.

The second theory states that the Payne effect is related to the matrix–filler interaction [82]. This theory is based on the idea of bound rubber that presents reduced molecular mobility and acts as supplementary crosslinks. With the strain amplitude increasing, a mechanism of adhesion and de-adhesion of polymer chains at the filler interface is proposed.

From the swelling experiment, Gauthier et al. [2] established that fillers immobilize nonvulcanized rubber since they avoid the migration of the bound rubber into the solvent. However, it is worth pointing out that although the models of the first type (infill structure models) can explain several aspects of the non-linear behavior of the filled rubber, they can barely explain the Payne effect. Meanwhile, it would reasonably not be correct to neglect the filler-filler interaction or the filler-polymer interaction.

The dynamic shear storage and loss moduli of all tested materials are reported in Figs. 7 and 10 respectively. Experimental data are represented by the curves in the shear strain amplitude range of about 0.02–10%, and they are interpolated by Kraus’s model (Equation 14 and Equation 15) in order to figure out the high strain amplitude plateau. As found by several authors [83–85], at strain amplitudes lower than 0.1% the storage modulus of filled rubbers reaches a plateau level named  $G'_0$ , while at high strain amplitudes (higher than 20%) it reaches a lower

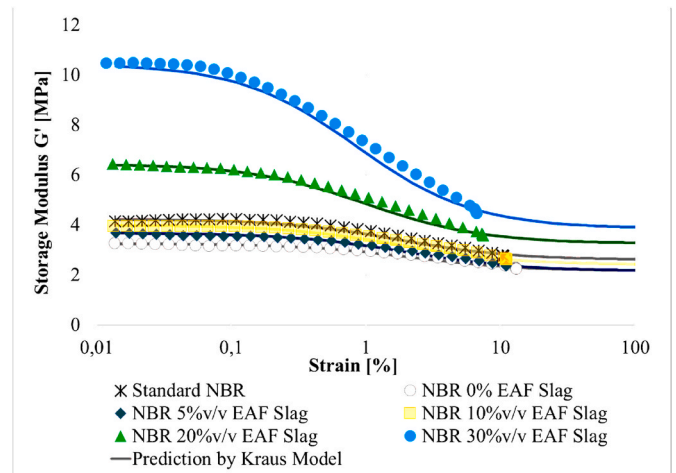


Fig. 7. Dynamic storage modulus in shear mode at 1 Hz, 23°C plotted against strain amplitude (0.02–10%) for Standard NBR and NBR filled with 0, 5 10 20 and 30% with EAF slag and application of Kraus model ( $G'(\gamma)$ ).

plateau value  $G'_{\infty}$  [64]. Kraus’s model storage and loss moduli curves are reported in Figs. 7 and 11 respectively up to a shear strain amplitude of 100%. It was found that Kraus’s model well represents the experimental data for the phenomenological exponent  $m$  fixed at 0.55.

It was found that the EAF slag as filler promotes a nonlinear dynamic behavior involving a storage modulus ( $G'$ ) reduction, by increasing the shear strain amplitude. This result was found to be in accordance with Ramorino et al. [64]. In particular, this behavior is more marked for a slag content higher than 20%v/v, while Standard NBR dynamic behavior was found to be very similar to that of NBR filled with EAF slag at 10%v/v. This is probably because in Standard NBR carbon black is more agglomerate and the calendaring process reduces the occluded rubber improving the distribution and the dispersion of carbon black. The better carbon black distribution for calendared NBR is observed by SEM images (Fig. 6).

It was found that by increasing the amount of EAF slag incorporated within the NBR matrix the Payne effect becomes more pronounced as shown in Fig. 8. The drop of the storage modulus with shear strain amplitude (Fig. 7) can be considered a measure of the Payne effect and it was found an increase of this effect with filler volume fraction according to many literature works [64,71,84–87]. Fig. 8 shows the influence of EAF slag volume fraction on the percentage change of the storage modulus from the low amplitude strain  $G'(\gamma_0)$  to the high amplitude strain plateaus  $G'_{\infty}$ .

It was found that the storage modulus of EAF slag filled NBR at 30%

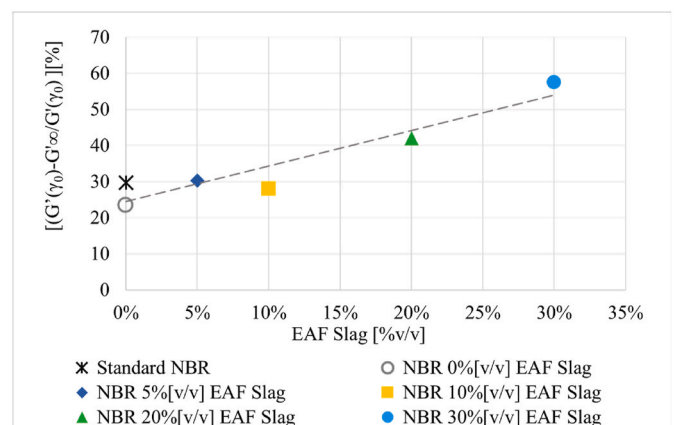


Fig. 8. Payne effect as Storage modulus variation [%] from low amplitude to high amplitude plateaus ( $G'(\gamma_0)$  and  $G'_{\infty}$ ) function of EAF slag volume fraction.

v/v is about the same as measured by Ramorino et al. [76] for natural rubber (SMR-GP) filled with organoclay at 20%wt.

Regarding the theoretical factors governing the storage modulus  $G'$ , it is possible to assume that at low strain amplitude, the predominant mechanism is filler-filler interaction, and with increasing the strain amplitude it turns out to be the rubber-filler interaction (bound rubber).

Nevertheless, at sufficient high strain (about 10%), where the filler network is believed to be fully destroyed,  $G'$  is proportional to the filler content showing the highest value for the highest EAF slag volume fraction. To explain this behavior, it is necessary to consider the hydrodynamic effect and the occluded rubber [88,89]. According to Medalia [89] the principal line of theoretical development has involved the treatment of the elastic modulus on a hydrodynamic basis, modified by the occluded rubber concept according to the Guth-Gold prevision model [58] that finds a good agreement with the experimental storage modulus at low strain amplitude as shown in Fig. 9. The rubber network contribution can be neglected for the purpose of evaluating the influence of filler particles in the NBR matrix because it can be assumed constant for all tested materials.

The loss modulus (Fig. 10) shows a loss peak at approximately the same dynamic amplitude range where the storage modulus is most rapidly decreasing. It is noteworthy that the peak of the loss modulus is much higher and occurs at lower strains as the filler volume fraction increases especially for NBR filled with EAF slag at 20 and 30%v/v. This could be explained by the presence of a layer of rigid rubber adherent to the filler particles that makes the compound stiffer and leads to an increase in the dissipation because the compound behavior will be more viscous. On the other hand, the dissipative phenomenon at the origin of the loss modulus peak is assumed to be the agglomeration and deagglomeration of the filler network which is consequently more marked and occurs at lower strain amplitude for higher filler volume fraction.

### 3.2.4. Crosslink density

Fig. 11 shows the swelling coefficient [%] and the crosslink density ( $\nu$  [mol/cm<sup>3</sup>]) determined by the Flory-Rehner equation (Equation (1) and Equation (2) respectively) for standard NBR and NBR composites filled with EAF slag in different amounts. It is observable that with increasing the EAF slag content in the NBR matrix the swelling coefficient decreases because the average molecular weight of the rubber segment between crosslinks  $M_c$  is reduced and consequently the crosslink density increases. This trend is in line with what is expected because it is reasonable to state that the immobilized rubber fraction around the slag particles is subjected to lower swelling, and by increasing this immobilized rubber fraction the average rubber crosslink density

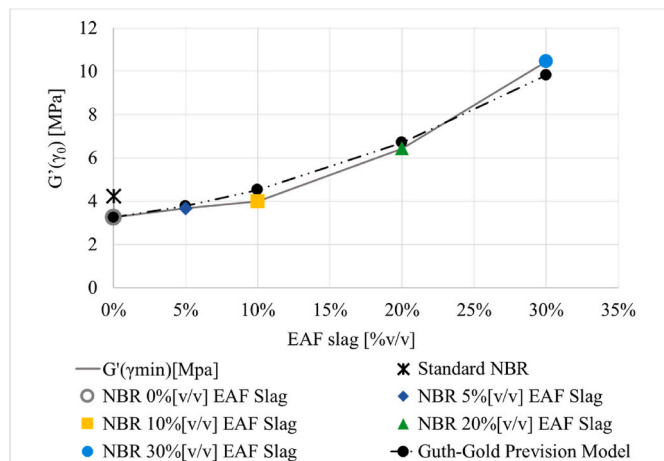


Fig. 9. Experimental and theoretical storage modulus at low strain amplitude  $G'(\gamma_0)$  function of EAF slag volume fraction.

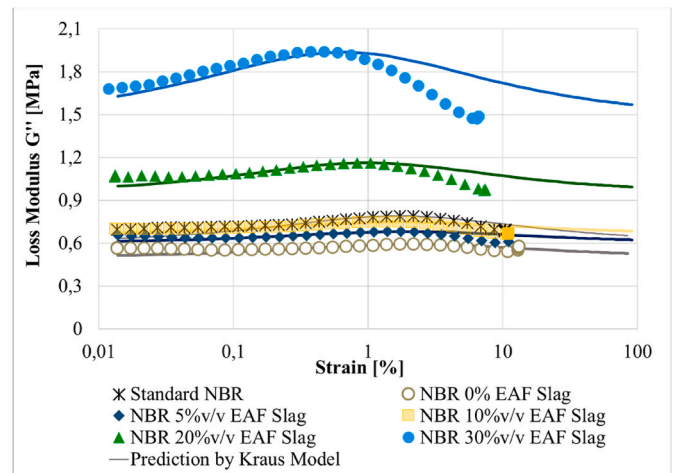


Fig. 10. Dynamic loss modulus in shear mode at 1 Hz, 23°C plotted against strain amplitude (0.02–10%) for Standard NBR and NBR filled with 0, 5, 10, 20 and 30% with EAF slag and application of Kraus model ( $G''(\gamma)$ ).

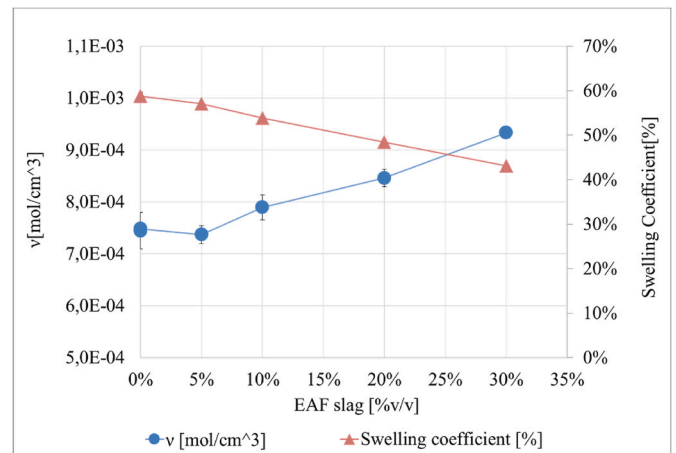


Fig. 11. Crosslink density determined by Flory-Rehner equation and swelling coefficient of Standard NBR and calendared NBR filled with 5, 10, 20, 30%v/v of EAF slag.

increases [3]. No differences are detected in the crosslink density of standard NBR and calendared NBR without EAF slag. This means the calendaring process does not affect the polymer's capability to vulcanize. This is probably due to two opposite phenomena: the better filler dispersion increases the carbon black surface area for the bound rubber formation, but on the other side the occluded rubber is reduced. The increase of crosslink density with EAF slag volume fraction due to the increase of bound rubber fraction [3] could be related to the general stiffening and strain at break reduction of NBR composites filled with slag. The increase in crosslink density as a function of slag content can be explained by contemplating the bound rubber around the filler surface [3,90–92].

Fig. 12 shows the plot of  $(V_{r0}/V_{rf})$  against  $(\phi/1-\phi)$  gives the extent of reinforcement (K) versus the filler volume fraction. The slope of the Kraus plot (K) is a measure of the polymer-filler interaction: the higher the negative slope value, the greater the reinforcement effect.  $V_{rf}$  is assumed equal to  $V_{r0}$  in order to evaluate the EAF slag influence neglecting that of carbon black which is constant for all the compounds. The ratio  $V_{r0}/V_{rf}$  is less than unity and the magnitude of the ratio decreases with filler loading, from a value of 1 for NBR without EAF slag to a value of 0.92 for EAF slag volume fraction of 30%, showing a reinforcement effect.

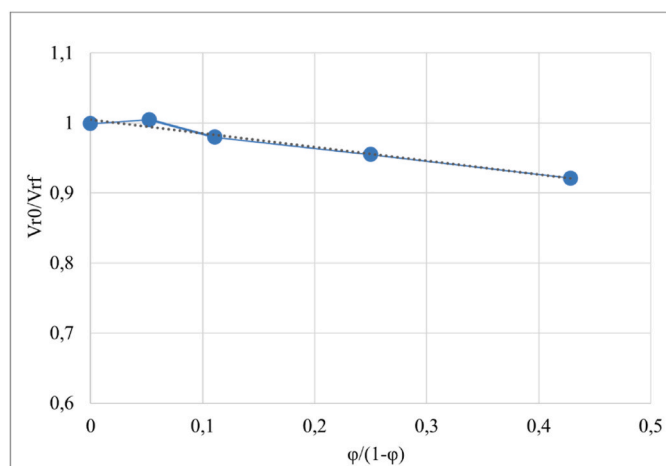


Fig. 12. Kraus plot of EAF slag filled NBR.

### 3.2.5. Differential scanning calorimetry analysis

The heat capacity increment,  $\Delta C_p^*$  as a measure of the amount of polymer which participates in the glass transition is dependent on the intermolecular rigidity, that is, the polymer–filler interaction in the filled rubber composites. The dependency  $\Delta C_p^*$  on intermolecular rigidity is estimated as immobilized polymer chains in the material. The immobilized rubber fraction was calculated according to Equation (6), the results are shown in Fig. 13. It is observable that with increasing the EAF slag content the heat capacity increment required by the rubber fraction in correspondence with the glass transition temperature decreases due to the presence of a rigid rubber fraction which remains in a glassy phase also above  $T_g$ .

## 4. Conclusion

In this research, the influence of EAF slag as filler for NBR matrix has been assessed according to experimental procedures and analytical calculations commonly adopted in evaluating the reinforcing effect of traditional fillers.

At first, the EAF slag employed as filler was characterized in terms of chemical composition by XRF, and phases by XRD and SEM/EDXS. One of the main critical issues in the safe reuse of the slag is the heavy metals leaching; in this study, it was found that thanks to the NBR's hydrophobicity, the leaching of Mo, Cr, and V is reduced by incorporating the slag particles into the rubber matrix.

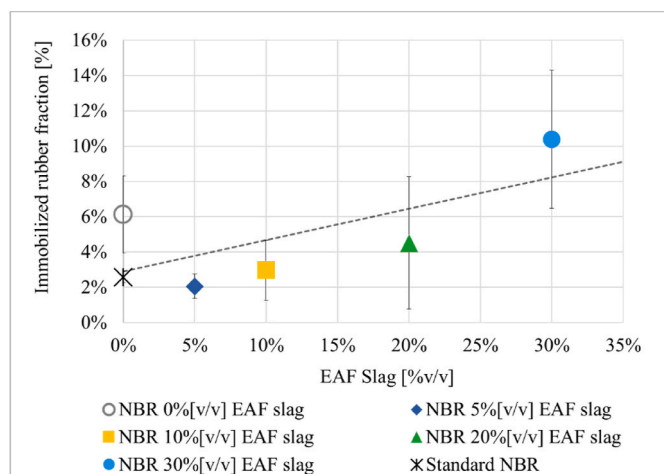


Fig. 13. Immobilized rubber fraction [%] of Standard NBR and calendered NBR filled with 5, 10, 20, 30%v/v of EAF slag.

As regards the compound characterization, it was found that the static and the dynamic properties of EAF slag filled NBR composites are affected by the slag content, in particular, in addition to an important contribution of the hydrodynamic effect, by the presence of a layer of rigid rubber around the filler particles (bound rubber) related to the filler-rubber interaction. With increasing the filler content, the immobilized rubber fraction quantified by DSC analysis increases as well as the crosslink density determined by the Flory-Rehner equation.

The hydrodynamic effect was evaluated on Young's modulus (E) determined by the tensile test and on the shear storage modulus ( $G'$ ) by DMA. It was found that the experimental data of E are well predicted by the Halpin-Tsai prevision model, while  $G'$  ( $\gamma_0$ ) by that proposed by Guth and Gold.

The presence of the EAF slag on the dynamic properties of NBR composites can be summarized as follow:

- The ability of NBR composites to storage and dissipate energy is evidenced by the storage and loss moduli curves shifted at higher modulus values proportionally to the amount of slag content.
- EAF slag increases the non-linear behavior (Payne effect): the immobilized rubber fraction increases so that the filler-matrix interaction contribute rises. The loss modulus peak occurs at approximately the same dynamic amplitude value where the storage modulus is most rapidly decreasing. The loss modulus peak is more marked and shifts towards smaller deformation amplitudes for high slag contents because the immobilized rubber fraction is greater, and the rigid layers of different particles come into contact with each other at lower strain amplitude.
- A good incorporation of the particles into the matrix was evident from the SEM observations.
- The glass transition temperature is not affected by the EAF slag content, this suggests the rubber-filler interaction force is not modified.

The present results show that the EAF slag could find a new field of applications promoting the circular economy in particular with the implementation of the industrial symbiosis where the industrial waste became input material for another industrial sector.

## Author contributions

Concept development (provided idea for the research), GR, GC, Design (planned the methods to generate the results), AG, Supervision (provided oversight, responsible for organization and implementation), GR, GC, Data collection/processing (responsible for experiments, patient management, organization, or reporting data), AG, Analysis/interpretation (responsible for statistical analysis, evaluation, and presentation of the results), AG, GC, GR, Literature search (performed the literature search), AG, Writing (responsible for writing a substantive part of the manuscript), AG, Critical review (revised manuscript for intellectual content, this does not relate to spelling and grammar checking), GC, GR, LED AZ, Other, M.L.M.

## Ethics approval and consent to participate

Not applicable.

## Consent for publication

Not applicable.

## Funding

None.

## Declaration of competing interest

The authors declare that they have no known competing financial interests or personal relationships that could have appeared to influence the work reported in this paper.

## Data availability

No data was used for the research described in the article.

## Acknowledgment

The authors thank Novotema S.p.A - Idex Corporation and Asonext Spa and for providing materials and test equipment for the composites characterization and acknowledge Lombardy Region and ENEA for the Ph.D. scholarship of AG.

## List of abbreviations

EAF	Electric Arc Furnace
NBR	Nitrile Butadiene Rubber
XRF	X-ray fluorescence
XRD	X-ray diffraction
SEM	Scanning Electron Microscopy
EDXS	Energy Dispersive X-ray Spectrometry
BSE	Back-scattered electron
G'	Shear storage modulus
G''	Shear dissipative modulus.

## References

- J.L. Valentín, I. Mora-Barrantes, J. Carretero-González, M.A. López-Manchado, P. Sotta, D.R. Long, K. Saalwächter, Novel experimental approach to evaluate Filler-Elastomer interactions, *Macromolecules* 43 (2010) 334–346, <https://doi.org/10.1021/ma901999j>.
- C. Gauthier, E. Reynaud, R. Vassoille, L. Ladouce-Stelandre, Analysis of the non-linear viscoelastic behaviour of silica filled styrene butadiene rubber, *Polymer* 45 (2004) 2761–2771, <https://doi.org/10.1016/j.polymer.2003.12.081>.
- S. Thomas, S.C. George, S. Thomas, Rigid amorphous phase: mechanical and transport properties of nitrile rubber/clay nanocomposites, *Prog. Rubber Plast. Recycl. Technol.* 33 (2017) 103–126, <https://doi.org/10.1177/147776061703300204>.
- V.P. Swapna, R. Stephen, T. Greeshma, C. Sharan Dev, M.S. Sreekala, Mechanical and swelling behavior of green nanocomposites of natural rubber latex and tubular shaped halloysite nano clay, *Polym. Compos.* 37 (2016) 602–611, <https://doi.org/10.1002/pc.23217>.
- L. Huang, F. Yu, Y. Liu, A. Lu, Z. Song, W. Liu, Y. Xiong, H. He, S. Li, X. Zhao, S. Cui, C. Zhu, Structural analyses of the bound rubber in silica-filled silicone rubber nanocomposites reveal mechanisms of filler-rubber interaction, *Compos. Sci. Technol.* 233 (2023), <https://doi.org/10.1016/j.compscitech.2022.109905>.
- L.A. Wilke, C.G. Robertson, D.A. Karsten, N.J. Hardman, Detailed understanding of the carbon black–polymer interface in filled rubber composites, *Carbon N. Y.* 201 (2023) 520–528, <https://doi.org/10.1016/j.carbon.2022.09.032>.
- S. Joly, G. Garnaud, R. Ollitrault, L. Bokobza, J.E. Mark, Organically modified layered silicates as reinforcing fillers for natural rubber, *Chem. Mater.* 14 (2002) 4202–4208, <https://doi.org/10.1021/cm020093e>.
- T. Goudarzi, D.W.D.W. Spring, G.H.G.H. Paulino, O. Lopez-Pamies, Filled elastomers: a theory of filler reinforcement based on hydrodynamic and interphasial effects, *J. Mech. Phys. Solid.* 80 (2015) 37–67, <https://doi.org/10.1016/j.jmps.2015.04.012>.
- L. Huang, F. Yu, Y. Liu, A. Lu, Z. Song, W. Liu, Y. Xiong, H. He, S. Li, X. Zhao, S. Cui, C. Zhu, Understanding the reinforcement effect of fumed silica on silicone rubber: bound rubber and its entanglement network, *Macromolecules* 56 (2023) 323–334, <https://doi.org/10.1021/acs.macromol.2c01969>.
- D. Mondal, S. Ghorai, D. Rana, D. De, D. Chattopadhyay, The rubber–filler interaction and reinforcement in styrene butadiene rubber/devulcanize natural rubber composites with silica–graphene oxide, *Polym. Compos.* 40 (2019) E1559–E1572, <https://doi.org/10.1002/pc.25076>.
- E. Guth, Theory of filler reinforcement, *J. Appl. Phys.* 16 (1945) 20–25, <https://doi.org/10.1063/1.1707495>.
- G. Tsagaropoulos, A. Eisenberg, Direct observation of two glass transition in silica-filled polymers. Implications for the morphology of random ionomers, *Macromolecules* 28 (1995) 396–398, <https://doi.org/10.1021/ma00105a059>.
- G. Tsagaropoulos, A. Eisenberg, Dynamic mechanical study of the factors affecting the two glass transition behavior of filled polymers. Similarities and differences with random ionomers, *Macromolecules* 28 (1995) 6067–6077, <https://doi.org/10.1021/ma00122a011>.
- M.-J. Wang, Effect of polymer-filler and filler-filler interactions on dynamic properties of filled vulcanizates, *Rubber Chem. Technol.* 71 (1998) 520–589, <https://doi.org/10.5254/1.3538492>.
- S. Merabia, P. Sotta, D.R. Long, A microscopic model for the reinforcement and the nonlinear behavior of filled elastomers and thermoplastic elastomers (Payne and Mullins Effects), *Macromolecules* 41 (2008) 8252–8266, <https://doi.org/10.1021/ma8014728>.
- S.-F. Li, X.-N. Wen, W.-L. Ju, Y.-L. Su, D.-J. Wang, Effects of particle-polymer interactions and particle-particle interactions on mechanical properties of polymer nanocomposites, *Acta Polym. Sin.* 52 (2021) 146–157, <https://doi.org/10.1177/j.issn1000-3304.2020.20189>.
- X. Shi, S. Sun, A. Zhao, H. Zhang, M. Zuo, Y. Song, Q. Zheng, Influence of carbon black on the Payne effect of filled natural rubber compounds, *Compos. Sci. Technol.* 203 (2021), <https://doi.org/10.1016/j.compscitech.2020.108586>.
- J. Plagge, A. Lang, Filler-polymer interaction investigated using graphitized carbon blacks: another attempt to explain reinforcement, *Polymer* 218 (2021), <https://doi.org/10.1016/j.polymer.2021.123513>.
- W.-G. Hwang, K.-H. Wei, C.-M. Wu, Mechanical, thermal, and barrier properties of NBR/organosilicate nanocomposites, *Polym. Eng. Sci.* 44 (2004) 2117–2124, <https://doi.org/10.1002/pen.20217>.
- S. Hosseini, S.M.S.M.S.M. Soltani, P.S. Fennell, T.S.Y. Choong, M.K. Aroua, Production and Applications of Electric-Arc-Furnace Slag as Solid Waste in Environmental Technologies: a Review, 2016, <https://doi.org/10.1080/21622515.2016.1147615>.
- N.M. Piatak, M.B. Parsons, R.R. Seal, Characteristics and environmental aspects of slag: a review, *Appl. Geochem.* 57 (2015) 236–266, <https://doi.org/10.1016/j.apgeochem.2014.04.009>.
- P. Ter Teo, A.S. Anasyida, M.S. Nurulakmal, Characterization of ceramic tiles added with EAF slag waste, *Adv. Mater. Res.* (2014), <https://doi.org/10.4028/www.scientific.net/AMR.1024.211>.
- M. Pisciotta, The volume expansion of artificial road aggregates derived from steelmaking slags, *Eur. Transp. - Trasp. Eur. Issue* 75, Paper n° 5, ISSN 1825-3997 (2020).
- S. Roy, S.I. Ahmad, M.S. Rahman, M. Salauddin, Experimental investigation on the influence of induction furnace slag on the fundamental and durability properties of virgin and recycled brick aggregate concrete, *Results Eng* 17 (2023), <https://doi.org/10.1016/j.rineng.2022.100832>.
- A. Diotti, L. Cominoli, A.P. Galvin, S. Sorlini, G. Plizzari, Sustainable recycling of electric arc furnace steel slag as aggregate in concrete: effects on the environmental and technical performance, *Sustain. Times* 13 (2021) 1–13, <https://doi.org/10.3390/su13020521>.
- L.H. Nguyen, T.D. Nguyen, T.V.N. Tran, D.L. Nguyen, H.S. Tran, T.L. Nguyen, T. H. Nguyen, H.G. Nguyen, T.P. Nguyen, N.T. Nguyen, Y. Ta, R. Sato, Steel slag quality control for road construction aggregates and its environmental impact: case study of Vietnamese steel industry—leaching of heavy metals from steel-making slag, *Environ. Sci. Pollut. Res.* 29 (2022) 41983–41991, <https://doi.org/10.1007/s11356-021-16438-1>.
- G. Cornacchia, S. Agnelli, M. Gelfi, G. Ramorino, R. Roberti, Reuse of EAF slag as reinforcing filler for polypropylene matrix composites, *JOM (J. Occup. Med.)* 67 (2015) 1370–1378, <https://doi.org/10.1007/s11837-015-1396-6>.
- A. Gobetti, G. Cornacchia, G. Ramorino, A. Riboldi, L.E. Depero, EAF slag as alternative filler for epoxy screeds , an example of green reuse, *Sustain. Mater. Technol.* 29 (2021), e00324, <https://doi.org/10.1016/j.jusmat.2021.e00324>.
- A. Gobetti, G. Cornacchia, C. Petrogalli, R.C. Kerschbaumer, M. La Monica, G. Ramorino, Characterization of recycled end-of-life rubber tire filled with black slag, *J. Reinforc. Plast. Compos.* (2023) 1–18, <https://doi.org/10.1177/07316844231155398>, 0.
- A. Gobetti, G. Cornacchia, G. Ramorino, Innovative reuse of electric arc furnace slag as filler for different polymer matrices, *Minerals* 11 (2021) 832, <https://doi.org/10.3390/min11080832>.
- A. Gobetti, G. Cornacchia, G. Ramorino, Reuse of Electric Arc Furnace slag as filler for nitrile butadiene rubber, *JOM (J. Occup. Med.)* (2022), <https://doi.org/10.1007/s11837-021-05135-6>.
- D.Y. Kim, J.W. Park, D.Y. Lee, K.H. Seo, Correlation between the crosslink characteristics and mechanical properties of natural rubber compound via accelerators and reinforcement, *Polymers* 12 (2020) 1–14, <https://doi.org/10.3390/polym12092020>.
- G. Heinrich, M. Klüppel, Recent advances in the theory of filler networking in elastomers, *Adv. Polym. Sci.* 160 (2002) 1–44, [https://doi.org/10.1007/3-540-45362-8\\_1](https://doi.org/10.1007/3-540-45362-8_1).
- C. Kraus, Interactions of elastomers and reinforcing fillers, *Rubber Chem. Technol.* 38 (1965) 1070–1114.
- M. Svanera, S. Panza, F. Uberto, R. Roberti, An innovative system for the re-use of slag from the Electric Arc Furnace | Un impianto innovativo nella filiera del recupero della scoria da forno elettrico, *La Metall. Ital.* 104 (2012) 37–43.
- R. Roberti, F. Uberto, M. Svanera, G. Altenburger, F. Cabra, The SLAG-REC® Project for an Innovative Direct Dry Granulation of EAF Slag, 2010.
- K.E. Daugherty, B. Saad, C. Weirich, A. Eberendu, The glass content of slag and hydraulic activity, *Silic. Ind.* 4 (5) (1983) 107–110.
- C. Navarro, M. Díaz, M.A. Villa-García, Physico-chemical characterization of steel slag. study of its behavior under simulated environmental conditions, *Environ. Sci. Technol.* 44 (2010), <https://doi.org/10.1021/es100690b>.
- CEN, I.S.O. CEN, EN 12457-2 Characterisation of Waste - Leaching - Compliance Test for Leaching of Granular Waste Materials and Sludges - Part 2: One Stage Batch Test at a Liquid to Solid Ratio of 10 L/kg for Materials with Particle Size below 4 Mm, without or with s, 2002, 12457-2.

- [40] A. Riboldi, G. Cornacchia, M. Gelfi, L. Borgese, A. Zacco, E. Bontempi, M. V. Boniardi, A. Casaroli, L.E. Depero, Grain size effect in elution test of electric arc furnace slag, *Appl. Sci.* 10 (2020), <https://doi.org/10.3390/app10020477>.
- [41] ISO 37, Rubber, Vulcanized or Thermoplastic — Determination of Tensile Stress-Strain Properties, 2017.
- [42] K.L. Mok, A.H. Eng, Characterisation of crosslinks in vulcanised rubbers: from simple to advanced techniques, *Malaysian J. Chem.* 20 (2018) 118–127.
- [43] F.A. Neugebauer, 9.1 Introduction, Nitrogen Oxy. Centered Radicals, 2006, pp. 7–9, [https://doi.org/10.1007/10858968\\_2](https://doi.org/10.1007/10858968_2).
- [44] K. Sridharan, K. Elangovan, Investigation on the swelling characteristics of NR/BR rubber blends, *J. Chem. Pharmaceut. Res.* 8 (2016) 553–557.
- [45] M. Barikani, C. Hepburn, Determination of crosslink density by swelling in the castable polyurethane elastomer based on 1/4 - cyclohexane diisocyanate and para-phenylene diisocyanate, Iran, *J. Polym. Sci. Technol.* 1 (1992) 1–5.
- [46] G.M. Bristow, W.F. Watson, Cohesive energy densities of polymers: Part 1. - cohesive energy densities of rubbers by swelling measurements, *Trans. Faraday Soc.* (1958), <https://doi.org/10.1039/TF9585401731>.
- [47] G.M. Bristow, W.F. Watson, Cohesive energy densities of polymers: Part 2. - cohesive energy densities from viscosity measurements, *Trans. Faraday Soc.* (1958), <https://doi.org/10.1039/TF9585401742>.
- [48] D.Y. Kim, J.W. Park, D.Y. Lee, K.H. Seo, Correlation between the crosslink characteristics and mechanical properties of natural rubber compound via accelerators and reinforcement, *Polymers* 12 (2020), <https://doi.org/10.3390/polym12092020>.
- [49] A. Sargsyan, A. Tonoyan, S. Davtyan, C. Schick, The amount of immobilized polymer in PMMA SiO<sub>2</sub> nanocomposites determined from calorimetric data, *Eur. Polym. J.* 43 (2007) 3113–3127, <https://doi.org/10.1016/j.eurpolymj.2007.05.011>.
- [50] D. Mombelli, A. Gruttadauria, S. Barella, C. Mapelli, The influence of slag tapping method on the efficiency of stabilization treatment of electric arc furnace carbon steel slag (EAF-C), *Minerals* 9 (2019), <https://doi.org/10.3390/min9110706>.
- [51] M. Tossavainen, F. Engstrom, Q. Yang, N. Menad, M. Lidstrom Larsson, B. Bjorkman, Characteristics of steel slag under different cooling conditions, *Waste Manag.* 27 (2007) 1335–1344, <https://doi.org/10.1016/j.wasman.2006.08.002>.
- [52] S. Çoruh, S. Eleveli, O.N. Ergun, G. Demir, Assessment of leaching characteristics of heavy metals from industrial leach waste, *Int. J. Miner. Process.* 123 (2013) 165–171, <https://doi.org/10.1016/j.minpro.2013.06.005>.
- [53] A. Król, K. Mizerna, The effect of particle size reduction of waste material on heavy metals release, *Chem* 69 (2015) 670–673.
- [54] Z. Guo, L. Zhang, Y. Cheng, X. Xiao, F. Pan, K. Jiang, Effects of pH, pulp density and particle size on solubilization of metals from a Pb/Zn smelting slag using indigenous moderate thermophilic bacteria, *Hydrometallurgy* 104 (2010) 25–31, <https://doi.org/10.1016/j.hydromet.2010.04.006>.
- [55] D.C. Edwards, Polymer-filler interactions in rubber reinforcement, *J. Mater. Sci.* (1990), <https://doi.org/10.1007/BF00581070>.
- [56] M.C.H. Lee, The effects of degree of mixing on the properties of filled elastomers, *J. Appl. Polym. Sci.* (1984), <https://doi.org/10.1002/app.1984.070290205>.
- [57] Q. Wang, F. Yang, Q. Yang, J. Chen, H. Guan, Study on mechanical properties of nano-Fe<sub>3</sub>O<sub>4</sub> reinforced nitrile butadiene rubber, *Mater. Des.* 31 (2010) 1023–1028, <https://doi.org/10.1016/j.matdes.2009.07.038>.
- [58] E. Guth, O. Gold, On the hydrodynamical theory of the viscosity of suspension, *Phys. Rev.* 53 (1938).
- [59] L. Petersson, K. Oksman, Biopolymer based nanocomposites: comparing layered silicates and microcrystalline cellulose as nanoreinforcement, *Compos. Sci. Technol.* 66 (2006) 2187–2196, <https://doi.org/10.1016/j.compscitech.2005.12.010>.
- [60] N. Ramasamy, A. Padmakumar, G. Haralur, N.K. Singha, Structure-property relationship of highly crosslinked rubber-iron oxide composite based on chloroprene rubber (CR) as well as on nitrile rubber (NBR); a comparative study using different models, *J. Macromol. Sci. Part A Pure Appl. Chem.* 58 (2020) 59–68, <https://doi.org/10.1080/10601325.2020.1826328>.
- [61] K. Roy, M.N. Alam, S.K. Mandal, S.C. Debnath, Effect of sol-gel modified nano calcium carbonate (CaCO<sub>3</sub>) on the cure, mechanical and thermal properties of acrylonitrile butadiene rubber (NBR) nanocomposites, *J. Sol. Gel Sci. Technol.* 73 (2015) 306–313, <https://doi.org/10.1007/s10971-014-3530-2>.
- [62] Q. Wang, F. Yang, Q. Yang, H. Guan, J. Chen, B. Zhao, Study on magnetic and physical mechanical properties of NBR composites filled with nano-SrO-6Fe<sub>2</sub>O<sub>3</sub>, *J. Elastomers Plastics* (2011), <https://doi.org/10.1177/0095244310393928>.
- [63] J.D. Ferry, Viscoelastic Properties of Polymers, 1980, <https://doi.org/10.1149/1.2428174>.
- [64] G. Ramorino, F. Bignotti, L. Conzatti, T. Ricco, Dynamic and viscoelastic behavior of natural rubber/layered silicate nanocomposites obtained by melt blending, *Polym. Eng. Sci.* (2007), <https://doi.org/10.1002/pen.20849>.
- [65] A.R. Payne, A note on the existence of a yield point in the dynamic modulus of loaded vulcanizates, *J. Appl. Polym. Sci.* 3 (1960), <https://doi.org/10.1002/app.1960.070030721>, 127–127.
- [66] L. Chazeau, J.D. Brown, L.C. Yanyo, S.S. Sternstein, Modulus recovery kinetics and other insights into the Payne effect for filled elastomers, *Polym. Compos.* 21 (2000) 202–222, <https://doi.org/10.1002/pc.10178>.
- [67] F. Schön, R. Thomann, W. Gronski, Shear controlled morphology of rubber/organoclay nanocomposites and dynamic mechanical analysis, *Macromol. Symp.* 189 (2002) 105–110, <https://doi.org/10.1002/masy.200290000>.
- [68] J.-T. Kim, T.-S. Oh, D.-H. Lee, Preparation and characteristics of nitrile rubber (NBR) nanocomposites based on organophilic layered clay, *Polym. Int.* 52 (2003) 1058–1063, <https://doi.org/10.1002/pi.1110>.
- [69] S. Varghese, J. Karger-Kocsis, K.G. Gatos, Melt compounded epoxidized natural rubber/layered silicate nanocomposites: structure-properties relationships, *Polymer* 44 (2003) 3977–3983, [https://doi.org/10.1016/S0032-3861\(03\)00358-6](https://doi.org/10.1016/S0032-3861(03)00358-6).
- [70] Y.T. Vu, J.E. Mark, L.H. Pham, M. Engelhardt, Clay nanolayer reinforcement of cis-1,4-polyisoprene and epoxidized natural rubber, *J. Appl. Polym. Sci.* 82 (2001) 1391–1403, <https://doi.org/10.1002/app.1976>.
- [71] A. Lion, C. Kardelky, P. Haupt, On the frequency and amplitude dependence of the Payne effect: theory and experiments, *Rubber Chem. Technol.* 76 (2003) 533–547, <https://doi.org/10.5254/1.3547759>.
- [72] S. Vieweg, R. Unger, K. Schroeter, E. Donth, G. Heinrich, Frequency and temperature dependence of the small-strain behavior of carbon-black filled vulcanizates, *Polym. Networks & Blends* 5 (1995) 199–204.
- [73] S. Vieweg, R. Unger, G. Heinrich, E. Donth, Comparison of dynamic shear properties of styrene-butadiene vulcanizates filled with carbon black or polymeric fillers, *J. Appl. Polym. Sci.* 73 (1999) 495–503, [https://doi.org/10.1002/\(SICI\)1097-4628\(19990725\)73:4<495::AID-APP5>3.0.CO;2-I](https://doi.org/10.1002/(SICI)1097-4628(19990725)73:4<495::AID-APP5>3.0.CO;2-I).
- [74] Z. Xu, Y. Song, Q. Zheng, Payne effect of carbon black filled natural rubber compounds and their carbon black gels, *Polymer* 185 (2019), <https://doi.org/10.1016/j.polymer.2019.121953>.
- [75] G. Ramorino, D. Vetturi, D. Cambiagli, A. Pegoretti, T. Ricco, Developments in dynamic testing of rubber compounds: Assessment of non-linear effects, *Polym. Test.* 22 (2003) 681–687, [https://doi.org/10.1016/S0142-9418\(02\)00176-9](https://doi.org/10.1016/S0142-9418(02)00176-9).
- [76] G. Ramorino, F. Bignotti, S. Pandini, T. Ricco, Mechanical reinforcement in natural rubber/organoclay nanocomposites, *Compos. Sci. Technol.* 69 (2009) 1206–1211, <https://doi.org/10.1016/j.compscitech.2009.02.023>.
- [77] M. Rendek, A. Lion, Amplitude dependence of filler-reinforced rubber: experiments, constitutive modelling and FEM - implementation, *Int. J. Solid Struct.* 47 (2010) 2918–2936, <https://doi.org/10.1016/j.ijsolstr.2010.06.021>.
- [78] A. Boonbumrung, P. Sae-Oui, C. Srisinha, Reinforcement of multiwalled carbon nanotube in nitrile rubber: in comparison with carbon black, conductive carbon black, and precipitated silica, *J. Nanomater.* 2016 (2016), <https://doi.org/10.1155/2016/6391572>.
- [79] A.R. Payne, The dynamic properties of carbon black-loaded natural rubber vulcanizates. Part I, *J. Appl. Polym. Sci.* 6 (1962) 57–63, <https://doi.org/10.1002/app.1962.070061906>.
- [80] A.I. Medalia, Morphology of aggregates. VI. Effective volume of aggregates of carbon black from electron microscopy: Application to vehicle absorption and to die swell of filled rubber, *J. Colloid Interface Sci.* 32 (1970) 115–131, [https://doi.org/10.1016/0021-9797\(70\)90108-6](https://doi.org/10.1016/0021-9797(70)90108-6).
- [81] A.I. Medalia, Elastic modulus of vulcanizates as related to carbon black structure, *Rubber Chem. Technol.* 46 (1973) 877–896, <https://doi.org/10.5254/1.3547416>.
- [82] M. Gerspacher, C.P. O'Farrell, H.H. Yang, C. Tricot, Modeling of the carbon black reinforcement mechanism in elastomers, *Rubber World* 214 (1996) 27–49.
- [83] F. Clément, L. Bokobza, L. Monnerie, Investigation of the Payne effect and its temperature dependence on silica-filled polydimethylsiloxane networks. Part I: experimental results, *Rubber Chem. Technol.* 78 (2005) 211–231, <https://doi.org/10.5254/1.3547879>.
- [84] G. Kraus, Reinforcement of elastomers by carbon black, *Angew. Makromol. Chem.* 60 (1977) 215–248, <https://doi.org/10.1002/apmc.1977.050600109>.
- [85] A.R. PAYNE, R.E. Whittaker, Low strain dynamic properties of filled rubbers, *Rubber Chem. Technol.* 44 (1971) 440–478, <https://doi.org/10.5254/1.3547375>.
- [86] L. Bokobza, O. Rapoport, Filled elastomers: mid- and near-IR spectroscopic determination of rubber dimensions in composite in unstretched state and under uniaxial extension, *J. Appl. Polym. Sci.* 87 (2002) 1204–1208, <https://doi.org/10.1002/app.11479>.
- [87] A.R. Payne, Dynamic properties of heat-treated butyl vulcanizates, *J. Appl. Polym. Sci.* 7 (1963) 873–885, <https://doi.org/10.1002/app.1963.070070307>.
- [88] C.M. Roland, Reinforcement of elastomers, *Ref. Modul. Mater. Sci. Mater. Eng.* (2016), <https://doi.org/10.1016/b978-0-12-803581-8.02163-9>.
- [89] A.I. Medalia, Effect of carbon black on dynamic properties of rubber vulcanizates, *Rubber Chem. Technol.* 51 (1978), <https://doi.org/10.5254/1.3535748>.
- [90] J. Berriot, F. Lequeux, L. Monnerie, H. Montes, D. Long, P. Sotta, Filler-elastomer interaction in model filled rubbers, a <sup>1</sup>H NMR study, *J. Non-Cryst. Solids* (2002) 307–310, [https://doi.org/10.1016/S0022-3093\(02\)01552-1](https://doi.org/10.1016/S0022-3093(02)01552-1), 719–724.
- [91] J. Berriot, H. Montes, F. Lequeux, D. Long, P. Sotta, Gradient of glass transition temperature in filled elastomers, *Europhys. Lett.* 64 (2003) 50–56, <https://doi.org/10.1209/epl/i2003-00124-7>.
- [92] J. Berriot, H. Montes, F. Lequeux, D. Long, P. Sotta, Evidence for the shift of the glass transition near the particles in silica-filled elastomers, *Macromolecules* 35 (2002) 9756–9762, <https://doi.org/10.1021/ma0212700>.